



OPEN

# DEP-CEEMDAN-MPE-INHT a time-frequency analysis method for noisy blasting seismic waves with adaptive noise suppression and endpoint processing

Miao Sun<sup>1,2</sup>, Jing Wu<sup>1,2</sup>✉, Yu-feng Wang<sup>3</sup>, Ya-ni Lu<sup>1</sup> & Fang-da Yu<sup>1</sup>

The Hilbert-Huang transform (HHT) is widely used for time-frequency analysis of blasting seismic wave signals due to its unique adaptability. However, blasting seismic wave signals are typical non-stationary vibration signals that are susceptible to noise interference, leading to mode confusion and endpoint effects in empirical mode decomposition (EMD) in HHT, which in turn affects the accuracy of time-frequency analysis. In order to obtain accurate time-frequency characteristic parameters of blasting seismic wave signals, it is necessary to improve HHT. A time-frequency analysis algorithm called DEP-CEEMDAN-MPE-INHT was proposed. The first step of the algorithm is to perform dual endpoint processing (DEP) on the signal. The second step is to combine the advantages of complete ensemble empirical mode decomposition with adaptive noise (CEEMDAN) and multi-scale permutation entropy (MPE) to obtain CEEMDAN-MPE, and perform CEEMDAN-MPE on the DEP processed signal to achieve synchronous suppression of high-frequency noise and low-frequency trend terms. The third step is to perform a normalized Hilbert transform (NHT) on the intrinsic mode function (IMF) obtained from DEP-CEEMDAN-MPE to achieve INHT. The above three steps can establish the time-frequency analysis algorithm of DEP-CEEMDAN-MPE-INHT. Through noisy simulation signal testing, the comparative study of DEP-CEEMDAN-MPE-INHT and HHT is carried out. Finally, the algorithm is applied to the time-frequency analysis of actual blasting seismic wave signals. The results show that DEP-CEEMDAN-MPE-INHT not only suppresses the EMD endpoint effect and mode confusion, but also obtains the time spectrum with high resolution in time domain and frequency domain. Through DEP-CEEMDAN-MPE-INHT time-frequency analysis, the time-frequency characteristic parameters of blasting seismic wave signal can be accurately extracted, which has important practical significance for the hazard identification and control of blasting seismic wave.

**Keywords** Blasting seismic wave signal, Empirical mode decomposition, Time-frequency analysis, Intrinsic mode function

With the rapid development of the national economy, blasting technology has been widely applied<sup>1</sup>. Blasting operations not only bring high efficiency, but also bring some negative effects, such as noise, dust, flying stones, and blasting seismic effects. The blasting seismic effect is known as the foremost hazard of blasting, and how to control the blasting seismic effect is currently an urgent problem to be solved<sup>2</sup>.

Time-frequency analysis is currently the widely used method for analyzing blasting seismic waves<sup>3</sup>. Common time-frequency analysis techniques include Fourier transform<sup>4</sup>, wavelet and wavelet packet analysis<sup>5</sup>, Wigner-Ville distribution<sup>6</sup>, and Hilbert-Huang transform (HHT)<sup>7</sup>. When Fourier transform is used to analyze non-stationary vibration signals, distortion of the results may occur<sup>8</sup>. Wavelet and wavelet packet algorithms can perform time-frequency analysis on blasting seismic wave signals, but it requires pre selection of wavelet basis functions. Different wavelet basis functions can obtain different analysis results and have multiple solutions<sup>9</sup>.

<sup>1</sup>School of Civil Engineering & Research Center of Hubei Small Town Development, Hubei Engineering University, Xiaogan 432000, China. <sup>2</sup>Engineering Research Center of Rock-Soil Drilling & Excavation and Protection, Ministry of Education, China University of Geosciences, Wuhan 430074, China. <sup>3</sup>Guangzhou Expressway Co., Ltd, Guangzhou 510335, China. ✉email: wujing@hbeu.edu.cn

When dealing with multi-component signals such as blasting seismic waves using the Wigner-Ville distribution, there may be interference from cross terms, which can sometimes seriously affect the original signal. Fourier transform and Wigner-Ville transform are both more suitable for stationary signals, and cannot provide accurate frequency domain features for non-stationary signal analysis<sup>5</sup>. HHT consists of two parts, empirical mode decomposition (EMD)<sup>10</sup> and Hilbert transform<sup>11</sup>. EMD decomposes the signal based on its time scale, and the frequency characteristics of the decomposed intrinsic mode function (IMF) are arranged in sequence from high frequency to low frequency, with each IMF having a clear physical meaning. Then, by performing Hilbert transform on the IMF, the time-frequency characteristic parameters of the blasting seismic wave signal can be obtained.

However, blasting seismic waves are susceptible to monitoring environment, testing systems, and human interference, resulting in the mixing of noise into the measured blasting seismic wave signal. The presence of noise will cause modal confusion and endpoint effects in EMD, thereby affecting the accuracy of time-frequency analysis. Modal confusion<sup>12</sup> is mainly caused by noise interference and manifests in two situations. The first scenario is when the same frequency distribution is in different IMF, while the second scenario is when different frequency distributions are in the same IMF. Endpoint effect<sup>13</sup> is an unavoidable phenomenon in the vast majority of signal processing. During signal decomposition, signals tend to deviate from the original signal at the endpoints. Noise interference will exacerbate the divergence phenomenon of signals at endpoints, so denoising the signal will effectively alleviate modal confusion and endpoint effects. Further consideration, constrained by the Bedrosian theorem, the traditional Hilbert transform will obtain negative instantaneous frequencies when dealing with IMF components with endpoint effects and mode confusion, making it difficult to identify the time-frequency characteristics of measured blasting seismic wave signals.

In order to obtain accurate time-frequency analysis results, it is necessary to improve HHT so that the improved algorithm can resist the interference of noise and achieve time-frequency analysis of blasting seismic wave signals mixed with noise<sup>14</sup>. The proposed DEP-CEEMDAN-MPE-INHT algorithm shares the same basic idea as advanced signal processing techniques such as ICEEMDAN (Improved Complete Ensemble Empirical Mode Decomposition with Adaptive Noise) and VMD (Variational Mode Decomposition) in enhancing the noise robustness of non-stationary signal analysis. At the same time, the DEP-CEEMDAN-MPE-INHT algorithm advances blasting seismic analysis by combining CEEMDAN's noise-adaptive framework with MPE's entropy-based denoising, outperforming ICEEMDAN in spectral separation while avoiding VMD's restrictive mode-number assumptions. Its innovative DEP component uniquely addresses persistent endpoint distortion issues, enabling more reliable extraction of physically interpretable time-frequency features from complex blast vibrations.

By comparing the time-frequency analysis of DEP-CEEMDAN-MPE-INHT and HHT using noisy simulated vibration signals, it was verified that DEP-CEEMDAN-MPE-INHT can obtain instantaneous frequencies with practical physical significance while suppressing EMD endpoint effects and modal confusion. Finally, the algorithm is applied to the time-frequency analysis of actual noisy blasting seismic wave signals. Research has found that this algorithm can effectively extract time-frequency characteristic parameters of noisy blasting seismic wave signals, achieve hazard identification of blasting seismic waves, and provide guidance for hazard control of blasting seismic waves.

## Principle of DEP-CEEMDAN-MPE-INHT time-frequency analysis method

### The principle of dual endpoint processing

The principle of empirical mode decomposition (EMD) to obtain intrinsic mode function (IMF) is to obtain the upper (lower) envelope of the signal according to all the maximum (small) value points of the signal  $S(t)$ , and then obtain the mean value satisfying the conditions through the "screening" of the upper and lower envelopes<sup>15</sup>. Because the end point of the signal is not necessarily the extreme point, the signal is easy to diverge when it is "filtered" to the end point, resulting in large error. The shorter the data contained in the signal, the greater the error<sup>16</sup>.

Relieve the divergence phenomenon of EMD at endpoints through dual endpoint processing (DEP). First level endpoint processing is to generate a sub wave  $S(t)_0$  through extreme value extension and calculate the energy of  $S(t)_0$ . Second level endpoint processing, adaptive energy matching, calculated using Eq. (1). Divide the original signal into  $x$  wavelets of the same length as  $S(t)_0$ , denoted as  $S(t)_1, S(t)_2, S(t)_3, \dots, S(t)_i, \dots, S(t)_x$  ( $1 \leq i \leq x$ ). Find a wavelet with the highest matching degree with  $S(t)_0$  energy, denoted as  $\hat{S}(t)_k$ , and translate  $S(t)_k$  to the endpoint to achieve dual endpoint processing (DEP).

$$\varepsilon = |E_0 - E_i| = \left| \int S_0^2(t) dt - \int S_k^2(t) dt \right| \quad (1)$$

In Eq. (1),  $\varepsilon$  represents the energy difference, and the smaller  $\varepsilon$ , the higher the matching degree between  $S(t)_0$  and  $S(t)_i$ . The  $S(t)_i$  corresponding to the minimum value of  $\varepsilon$  is  $S(t)_k$ . Figure 1 is the operation flow chart of DEP.

### The principle of CEEMDAN-MPE

The core of CEEMDAN-MPE algorithm is to suppress EMD modal confusion by reducing noise. CEEMDAN-MPE utilizes the randomness detection capability of multi-scale permutation entropy (MPE)<sup>17</sup> to suppress high-frequency noise, optimize EMD to obtain complete ensemble empirical mode decomposition with adaptive noise (CEEMDAN)<sup>18,19</sup>, which has good control over low-frequency trend terms. By combining the advantages of CEEMDAN and MPE, blasting seismic wave denoising can be achieved.

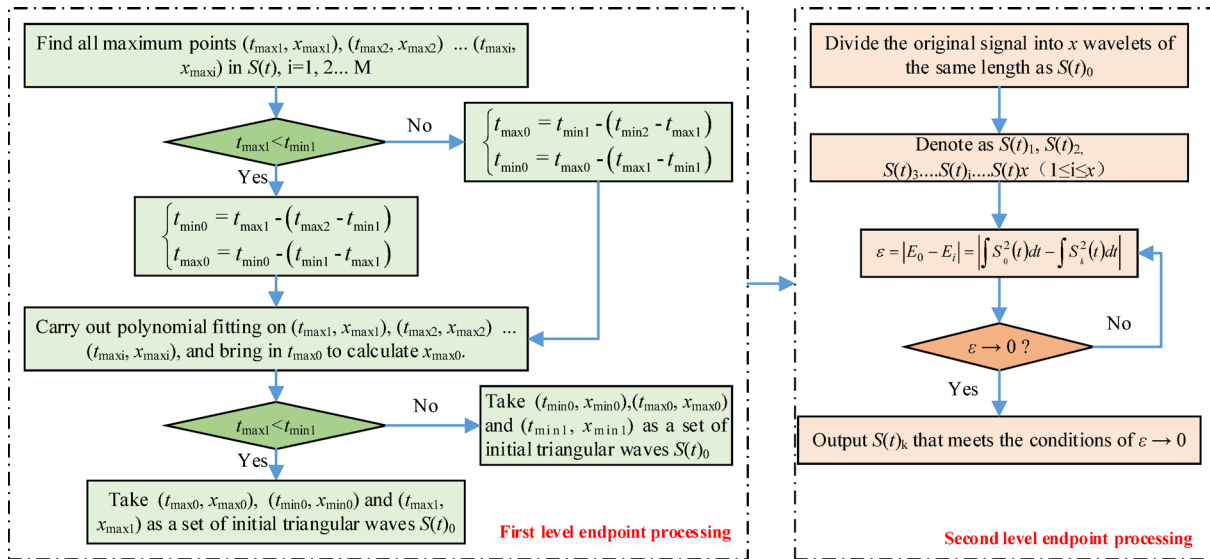


**Fig. 1.** Dual endpoint processing flow chart.

CEEMDAN adds finite times of adaptive white noise in each stage of decomposition, which can achieve almost zero reconstruction error with less average times. The specific steps are as follows:

Step 1: Add the adaptive white noise  $B_j(t)$  to the signal  $S(t)$  after the DEP, where  $j$  is the number of times to add the noise, 50 times in this paper. Then, the  $j$ -th order signal can be represented by Eq. (2).

$$S(t) = S(t) + \alpha_j \cdot B_j(t) \quad (j = 1, 2, \dots, N) \quad (2)$$

Among them:  $S(t)$  is the signal after adding noise for the  $j$ th time.  $\alpha_j$ : The standard deviation of the  $j$ th addition of  $B_j(t)$ .  $B_j(t)$ : The  $j$ th addition of adaptive white noise.  $N$ : Total number of additions ( $N = 50$ ).

For the IMF1 obtained by CEEMDAN, see Eq. (3), where the remainder  $R_1(t) = S(t) - \text{IMF1}$ .

$$\text{IMF1} = \frac{1}{N} \sum_{j=1}^N \text{IMF1}^j \quad (3)$$

Step 2: Perform EMD on the new signal  $S(t) = R_1(t) + \alpha_j^* B_j(t)$ , extract the first-order intrinsic mode function, and take the overall average of the obtained first-order intrinsic mode function to obtain IMF2. At this point, the remaining term  $R_2(t) = S(t) - \text{IMF2}$ .

Step 3: Repeat “Step2” until the end of the program.  $S(t)$  gets  $c$  IMF and the unique remainder  $R(t)$  through CEEMDAN. The decomposition result is shown in Eq. (4).

$$R(t) = S(t) - \sum_{i=1}^c \text{IMF}_i \quad (4)$$

The advantage of multi-scale permutation entropy (MPE) over permutation entropy (PE)<sup>20</sup> lies in its multi-scale coarse-grained processing, which segments the time series (in this paper, the IMF obtained from DEP-CEEMDAN) and averages them in each segment to further improve processing accuracy. By setting the permutation entropy threshold, the entropy value of the processed time series can be controlled to suppress the high-frequency noise mixed in the vibration signal during monitoring. The operation process of CEEMDAN-MPE is analyzed only through the flow chart, and Fig. 2 is the operation flow chart of CEEMDAN-MPE.

### The principle of INHT

Hilbert transform to obtain the instantaneous frequency with physical significance usually requires IMF to meet more stringent conditions. Blasting seismic wave, a complex multi-component signal, can not meet the demand of IMF obtained by EMD directly, which will lead to the loss of significance of Hilbert transform. Based on this, Huang proposed that Normalized Hilbert Transform (NHT) makes Hilbert transform free from Bedrosian theorem constraints<sup>21</sup>. However, the IMF used for NHT comes from EMD or ensemble empirical mode decomposition (EEMD). As mentioned above, the inherent modal confusion and endpoint effect of EMD lead to the unstable IMF; EEMD suppresses modal confusion by adding random white noise, which can not prove that random noise has no impact on the integrity of the original signal, nor can it solve the endpoint effect. The IMF used for NHT in this paper is obtained by DEP-CEEMDAN-MPE, which has carried out EMD mode confusion and endpoint processing, so it is called Improved Normalized Hilbert Transform (INHT).

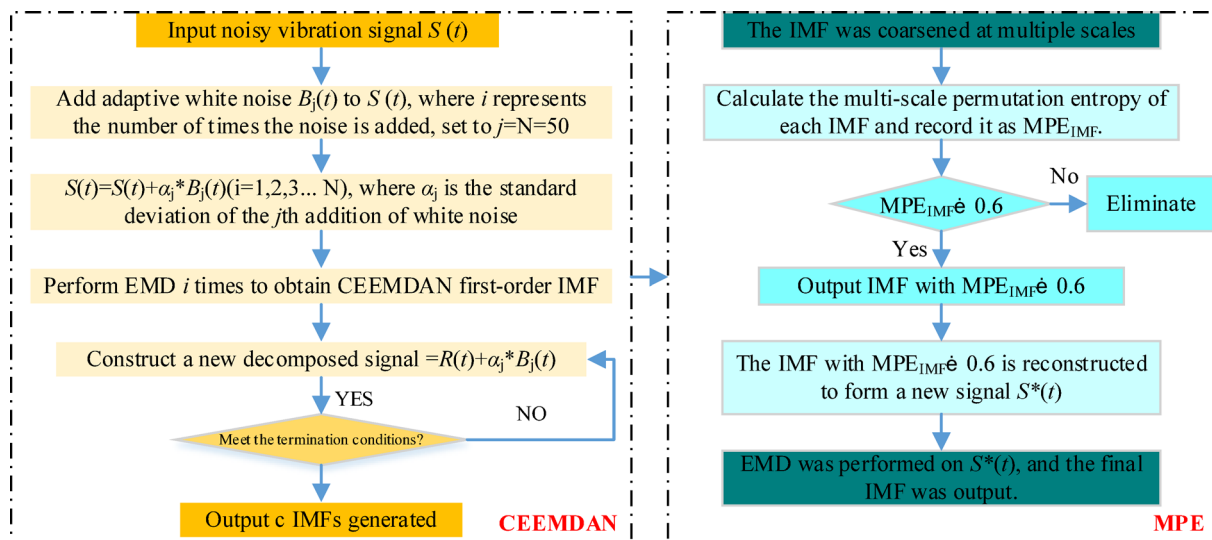


**Fig. 2.** CEEMDAN-MPE algorithm flow chart.

The specific operation of INHT is as follows:

Step 1: Take the absolute value of IMF obtained by DEP-CEEMDAN-MPE, and find out all the maximum values in the absolute value of IMF.

Step 2: Get the spline envelope of the maximum point of the absolute value of IMF, and record it as  $x(t)$ .

Step 3: Normalization processing, record the spline envelope of all maximum points in the absolute value of IMF1 as  $x_1(t)$ , and calculate  $f_1(t) = \text{IMF1}/x_1(t)$ .

Step 4: if all  $|f_1(t)|$  satisfy  $|f_1(t)| \leq 1$ , stop. On the contrary, re assign the value of IMF1, make  $\text{IMF1} = f_1(t)$ , repeat "Step 2" to get the spline envelope of all the maximum points in  $|f_1(t)|$  and record it as  $x_2(t)$ , repeat "the third step" to get  $f_2(t) = f_1(t)/x_2(t)$ , and check whether  $|f_2(t)|$  meets  $|f_2(t)| \leq 1$ , see Eq. (5) for details, where  $d$  is the number of repetitions, and generally 2~3 times can meet the demand. IMF2, IMF3 and IMF $i$  calculations are the same as IMF1.

$$\left\{ \begin{array}{l} f_1(t) = \text{IMF1}/x_1(t) \\ f_2(t) = f_1(t)/x_2(t) \\ f_3(t) = f_2(t)/x_3(t) \\ \vdots \\ f_d(t) = f_{d-1}(t)/x_d(t) \end{array} \right. \quad (5)$$

In Eq. (5),  $f_d(t)$  is the frequency modulation part of IMF1. Therefore, the normalized IMF1 can be expressed by Eq. (6). In Eq. (6),  $w_d(t)$  is the amplitude modulation part of IMF1.

$$\text{IMF } f_d(t) \cdot w_d(t) \quad (6)$$

Step 5: Hilbert transform  $f_d(t)$ , see Eq. (7).

$$\text{Hilber}[f_d(t)] = \frac{1}{\pi} \int_{-\infty}^{+\infty} \frac{f_d(\tau)}{t - \tau} d\tau \quad (7)$$

The phase function  $\theta(t)$  of IMF1 is obtained by using arctangent function. See Eq. (8).

$$\theta(t) = \arctan \frac{\text{Hilber}[f_d(t)]}{f_d(t)} \quad (8)$$

The instantaneous frequency  $\omega(t)$  can be obtained by deriving  $\theta(t)$ . The expression of  $\omega(t)$  is shown in Eq. (9).

$$\omega(t) = \frac{1}{2\pi} \frac{d\theta(t)}{dt} \quad (9)$$

In Eq. (9) the  $\omega(t)$  is the instantaneous frequency of IMF1, which has practical physical significance. Similarly, the instantaneous frequency of any IMF can be obtained.

To better understand the algorithm principle, draw a flowchart of the DEP-CEEMDAN-MPE-INHT time-frequency analysis method, as shown in Fig. 3.

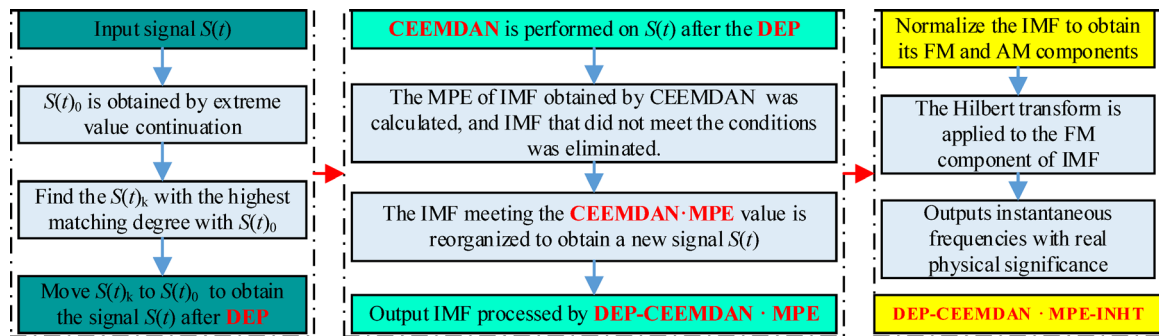


**Fig. 3.** DEP-CEEMDAN-MPE-INHT algorithm flow chart.

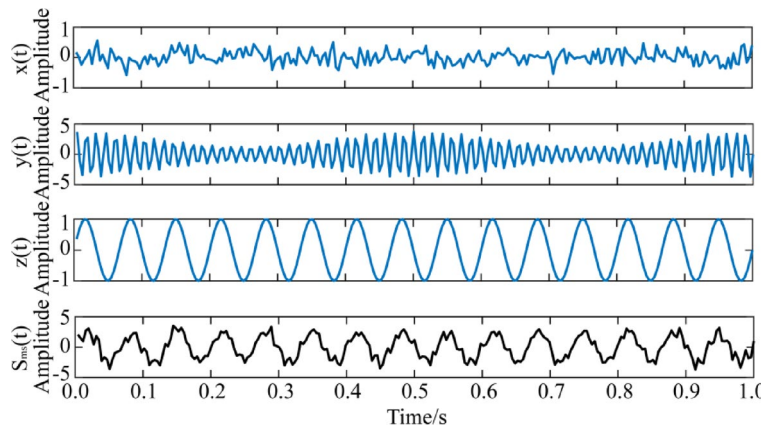


**Fig. 4.**  $S_{ms}(t)$  and its components.

### Time frequency analysis of noisy simulation vibration signal

#### Establish a noisy simulation vibration signal

The DEP-CEEMDAN-MPE-INHT algorithm is applied to the time-frequency analysis of noisy simulation vibration signal ( $S_{ms}(t)$ ), and the time-frequency analysis results of DEP-CEEMDAN-MPE-INHT algorithm and HHT algorithm are compared and analyzed to highlight the advantages of DEP-CEEMDAN-MPE-INHT in processing noisy signals.

$S_{ms}(t) = x(t) + y(t) + z(t)$ , where  $x(t)$  is the gauss white noise with power equal to 0.1;  $y(t) = (1 + 0.5 \times \cos(2\pi \times 2t)) \times \sin(2\pi \times 70 \times t + 2\pi \times t^2)$  is an amplitude modulation/frequency modulation signal;  $z(t) = \sin(2\pi \times 15 \times t)$  is the sinusoidal signal with frequency equal to 15. The number of sampling points  $N = 256$  and time series  $t = 1/N:1/N:1$ .  $S_{ms}(t)$  and its components are shown in Fig. 4.

#### Comparative study on time-frequency analysis of noisy simulation vibration signal DEP-CEEMDAN-MPE-INHT and HHT

##### Decomposition results of noisy simulation vibration signal

The decomposition results of noisy simulation vibration signal by EMD and DEP-CEEMDAN-MPE are shown in Fig. 5. Figure 5a shows EMD results. It can be found that high-frequency mode confusion is very serious, such as IMF1. The intermediate frequency is relatively stable, such as IMF2 and IMF3, but divergence appears at the left endpoint of IMF2. Low-frequency endpoints diverge more seriously. For example, IMF4 shows a trend of low-frequency development at right endpoints. Figure 5b shows the results of DEP-CEEMDAN-MPE. The decomposition results are arranged from high frequency to low frequency, and the mode confusion and endpoint effect caused by EMD are effectively suppressed.

##### Comparative analysis of noisy simulation vibration signal HT and INHT

Hilbert transform and INHT were performed on IMF in Fig. 5a and b respectively to obtain two-dimensional time-frequency spectrum of a single IMF. The transformation results are shown in Fig. 6a and b. We ignore the remainder  $R(t)$  here.

In the noisy simulation vibration signal,  $y(t)$  is an amplitude modulation/frequency modulation signal with a frequency of about 70 Hz.  $z(t)$  is a sinusoidal signal with a frequency of 15 Hz. By observing Fig. 6a, it is not difficult to find that due to the interference of white noise  $x(t)$ , the time-frequency spectrum of IMF1 obtained by EMD are seriously confused by Hilbert transform. During the whole Hilbert transform process, the frequency of IMF1 always oscillates between 50 Hz and 150 Hz, and the high-frequency modes are seriously confused.

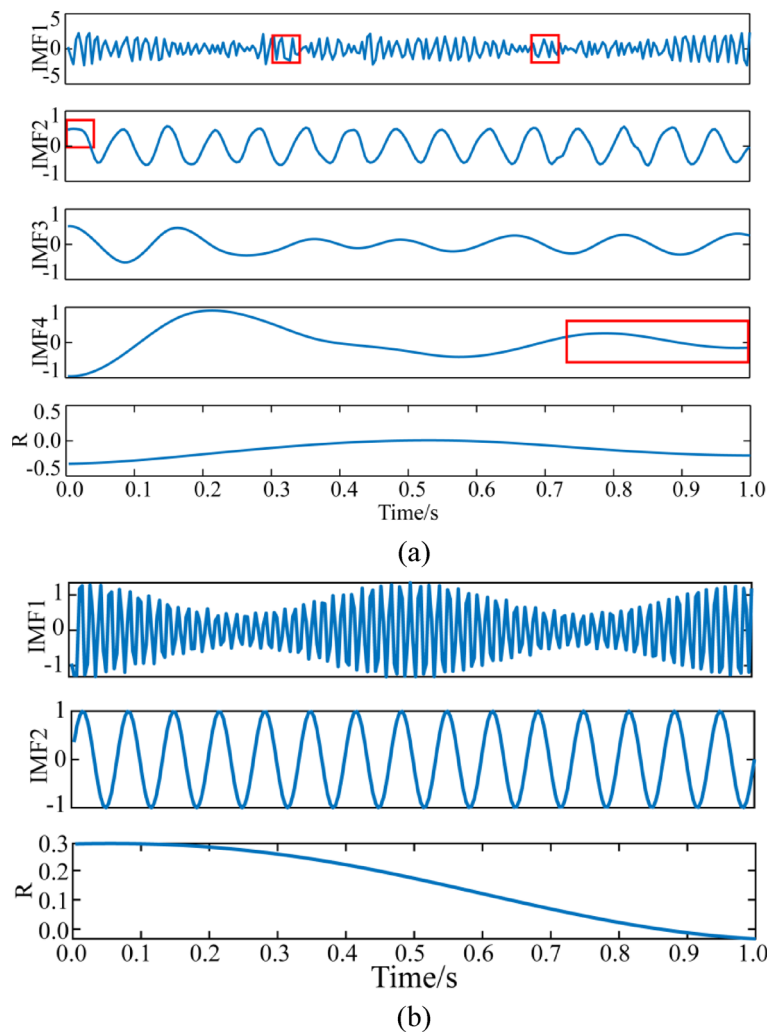


**Fig. 5.** IMF from EMD and DEP-CEEMDAN-MPE. **(a)** EMD decomposition results. **(b)** DEP-CEEMDAN-MPE decomposition results.

The middle and low frequencies are relatively stable, which is consistent with the analytical conclusion obtained in Fig. 5a. Comparing Figs. 5a and 6a, it can be found that there is a one-to-one correspondence between IMF component and time-frequency spectrum. Taking IMF4 as an example, the frequency at the left endpoint is higher than that at the right endpoint, and the IMF plot obtained at Fig. 5a and the time-frequency spectrum plot obtained at Fig. 6a both show consistent results.

In Fig. 6b, the single IMF time-frequency spectrum obtained by DEP-CEEMDAN-MPE can be found that the results of time-frequency analysis can accurately extract the time-frequency characteristics of noisy simulation signals on the premise of suppressing EMD mode confusion and endpoint effect. IMF1 corresponds to  $y(t)$ . IMF2 corresponds to  $z(t)$ ; The interference caused by  $x(t)$  is suppressed. The IMF component obtained from Fig. 5b also has a one-to-one correspondence with the time-frequency spectrum obtained from Fig. 6b.

#### Time frequency analysis results of noisy simulated vibration signal

Through time-frequency analysis comparative study of noisy simulated vibration signal, the following conclusions can be drawn:

- 1) The IMF component obtained by DEP-CEEMDAN-MPE is more stable than EMD, and modal confusion and endpoint effect are effectively suppressed.
- 2) INHT is a normalized Hilbert transform applied to the IMF obtained from DEP-CEEMDAN-MPE, suppressing endpoint effects and mode confusion. The resulting time-frequency spectrum is clearer in physical meaning and more accurate in time-frequency distribution compared to HHT.
- 3) Comparing the stability of IMF components and the accuracy of time-frequency spectrum, DEP-CEEMDAN-MPE is more suitable for time-frequency analysis of noisy vibration signals compared to HHT.

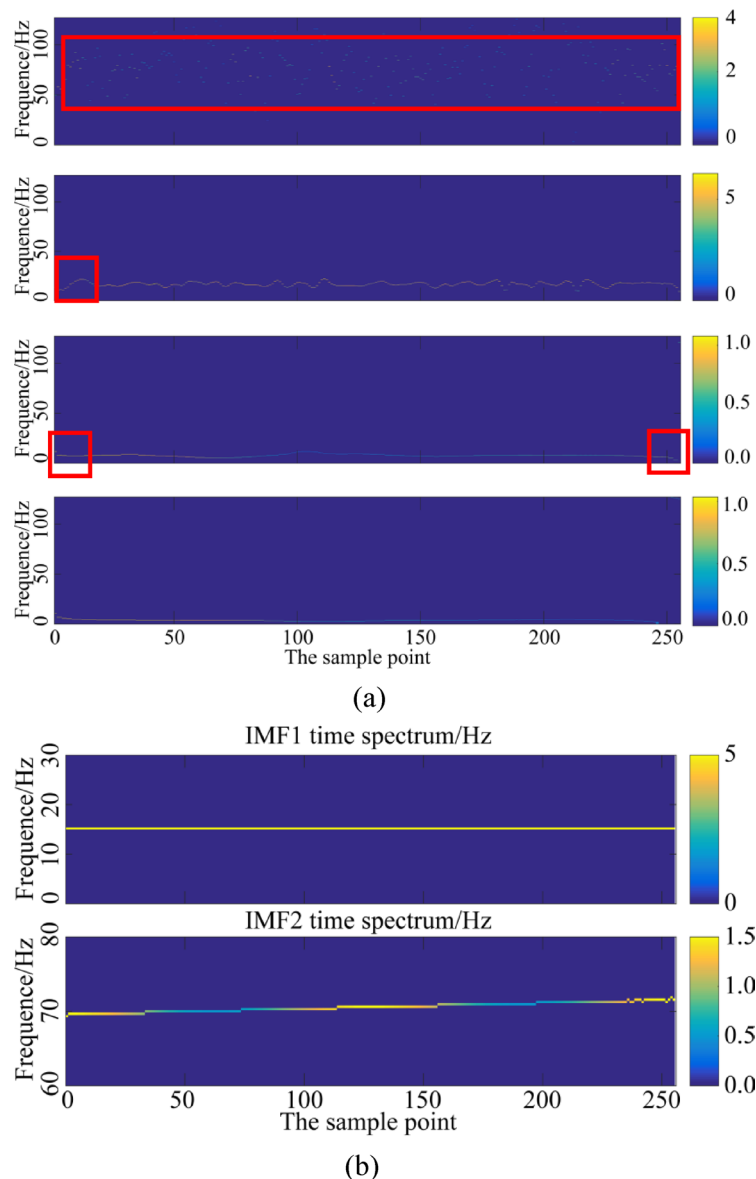


**Fig. 6.** Time-frequency spectrum of a single IMF. (a) Time-frequency spectrum obtained by HT. (b) Time-frequency spectrum obtained by INHT.

#### Case study: Time-frequency analysis of blasting seismic wave signals containing noise based on DEP-CEEMDAN-MPE-INHT

##### Actual project overview

Taking the reef blasting project in LT7 area at shaijingping in Liantuo section between the Three Gorges and Gezhouba dams as the research object, LT7 area has large reef thickness, the deepest drilling depth, great construction difficulty and complex surrounding environment. Figure 7 is the construction plan of reef blasting regulation project in LT7 area. It can be seen from Fig. 7 that LT7 is divided into three construction areas (area A, area B and area C). The areas with thick blasting layer are mainly concentrated in area C.

Through the above analysis, it can be seen that the construction in area C has the greatest relative impact during the construction in area LT7. During the construction period, the blasting area is about 200 m away from the important structure-Liantuo Bridge. Whether the blasting effect will cause resonance damage to Liantuo Bridge is a key issue that needs to be paid attention to in this blasting construction.

The TC-4850 blasting vibration meter was used to monitor the Liantuo Bridge, and a typical blasting vibration signal from the monitoring point was selected as the research object, as shown in Fig. 8.

##### Time frequency analysis of blasting seismic wave signals containing noise

Perform time-frequency analysis on the measured signal in Fig. 8 using DEP-CEEMDAN-MPE-INHT. In the first step, decompose signal by DEP-CEEMDAN-MPE algorithm to obtain IMF components as shown in Fig. 9. It can be found that IMF is arranged from high frequency to low frequency, and there is no obvious modal

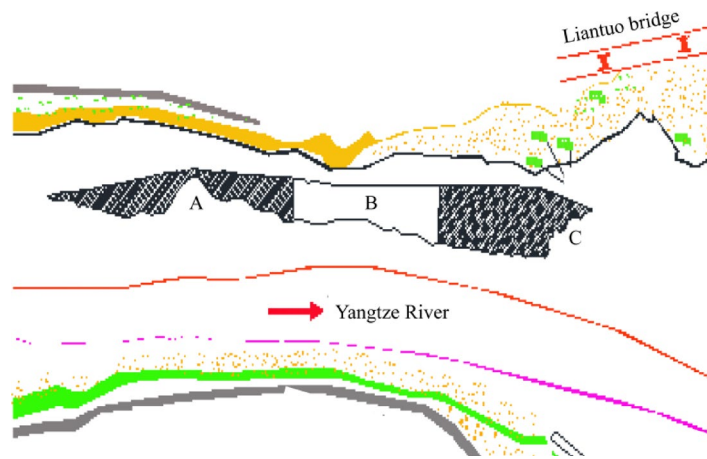


**Fig. 7.** Construction plan of reef blasting project in LT7.

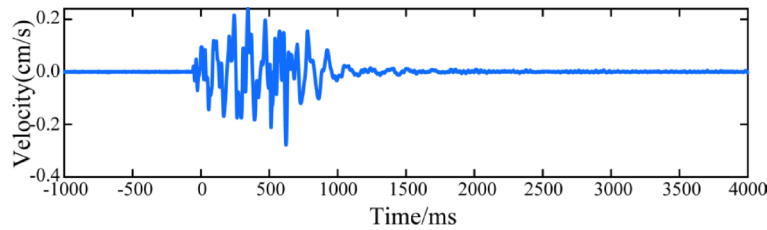


**Fig. 8.** The waveform of the actual blasting seismic wave monitoring signal.

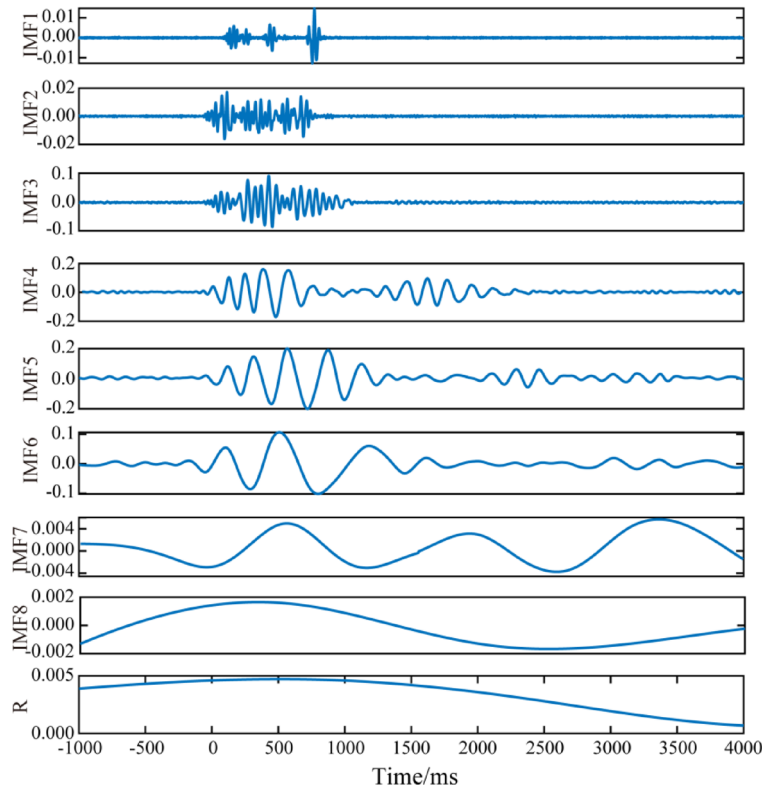


**Fig. 9.** IMF based on DEP-CEEMDAN-MPE.

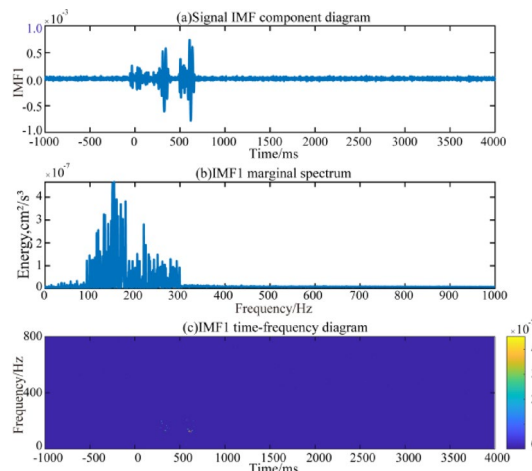


**Fig. 10.** IMF1 time-frequency energy characteristic diagram.

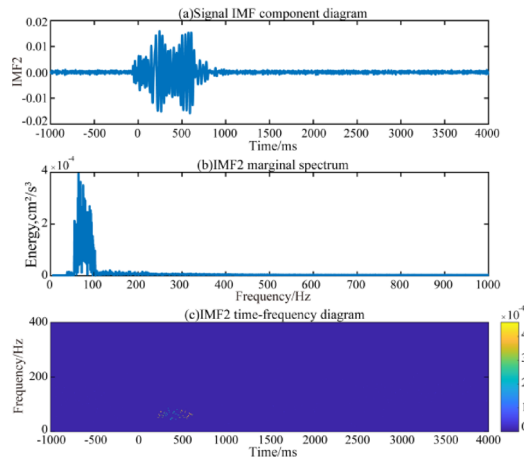


**Fig. 11.** IMF2 time-frequency energy characteristic diagram.

confusion and endpoint effect. Each IMF carries a set of specific frequency information of blasting seismic wave signal. IMF1 is the decomposed high-frequency component; IMF2 and IMF3 are the intermediate frequency components of this decomposition; IMF4-IMF7 are the low-frequency components of this decomposition;  $R$  is the remainder.

Further analysis, INHT is performed on the IMF in Fig. 9 to obtain the time-frequency energy characteristic diagram of a single IMF as shown in Figs. 10, 11, 12, 13, 14, 15 and 16. The corresponding figure (a) is a single IMF; (b) Figure is the marginal spectrum of a single IMF; (c) The figure is the time-frequency spectrum of a single IMF, and the remainder  $R$  is ignored here. Energy analysis based on marginal spectrum (Figs. 10b, 11, 12, 13, 14 and 15b) confirms that IMF2-IMF4 carry the highest energy density, while IMF5-IMF6 exhibit lower energy despite their larger time-domain amplitudes.

It can be found from Figs. 10, 11, 12, 13, 14, 15 and 16 that the time-frequency energy characteristic diagram obtained by DEP-MPE-CEEMDAN-INHT has high resolution in both time domain and frequency domain. The frequency range of IMF1 is 100–300 Hz and the duration is 0.35–0.60 s; the frequency range of IMF2 is 50–100 Hz and the duration is 0.25–0.60 s; the frequency range of IMF3 is 20–50 Hz and the duration is 0.00–1.00 s; the frequency range of IMF4 is 10–25 Hz and the duration is 0.00–1.90 s; the frequency range of IMF5 is 5–10 Hz and the duration is 0.00–1.45 s; the frequency range of IMF6 is 2–5 Hz and the duration is 0.55–4.00 s; the frequency of IMF7 is the lowest, about 0–2 Hz, and the duration is 0.00–3.30 s.

By analyzing Figs. 10, 11, 12, 13, 14, 15 and 16, it can be found that the signal energy is mainly concentrated in IMF2-IMF4. The three-dimensional time frequency energy spectrum of signal in Fig. 8 is further analyzed, as shown in Fig. 17. Observing Fig. 17, it can be found that the signal energy is mainly concentrated in the time range of 0.20–0.80 s, mainly distributed below 70 Hz, especially in the range of 2–40 Hz. Further analysis shows that the main frequency of signal is 10.50 Hz and the secondary main frequency is 6.41 Hz.

According to the knowledge of structural earthquake resistance, when the frequency of blasting seismic wave is the same as the natural frequency of the house, the amplitude of the structure will reach the maximum, that

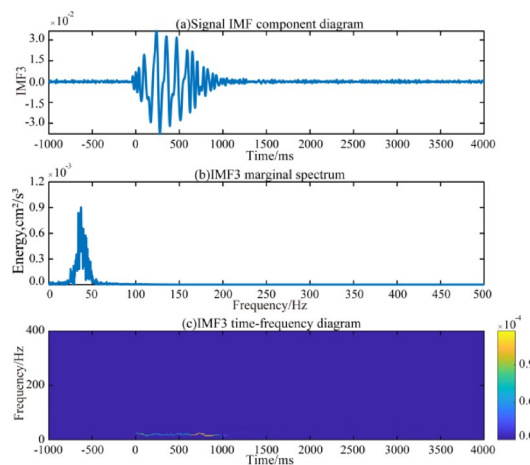


**Fig. 12.** IMF3 time-frequency energy characteristic diagram.

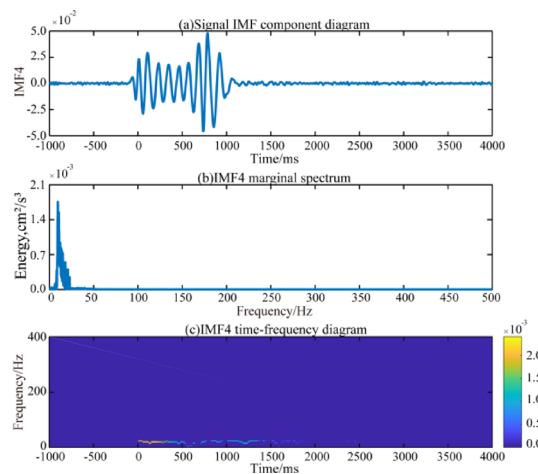


**Fig. 13.** IMF4 time-frequency energy characteristic diagram.

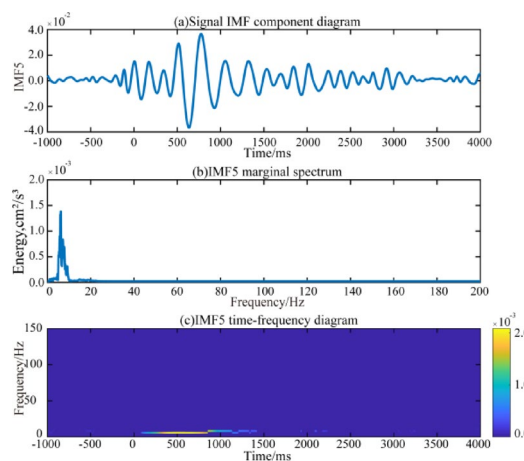


**Fig. 14.** IMF5 time-frequency energy characteristic diagram.

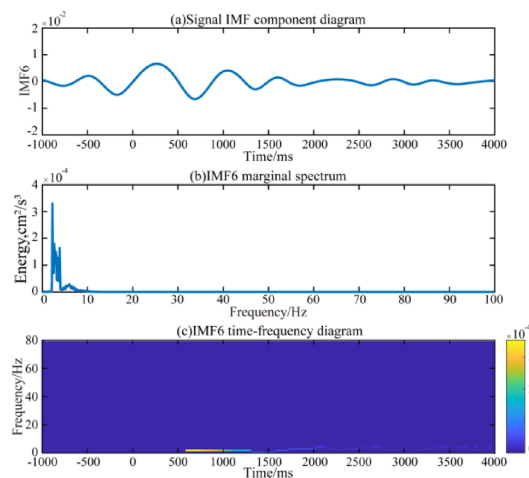


**Fig. 15.** IMF6 time-frequency energy characteristic diagram.

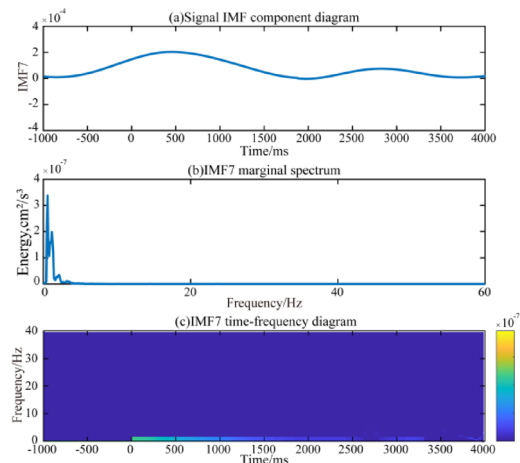


**Fig. 16.** IMF7 time-frequency energy characteristic diagram.

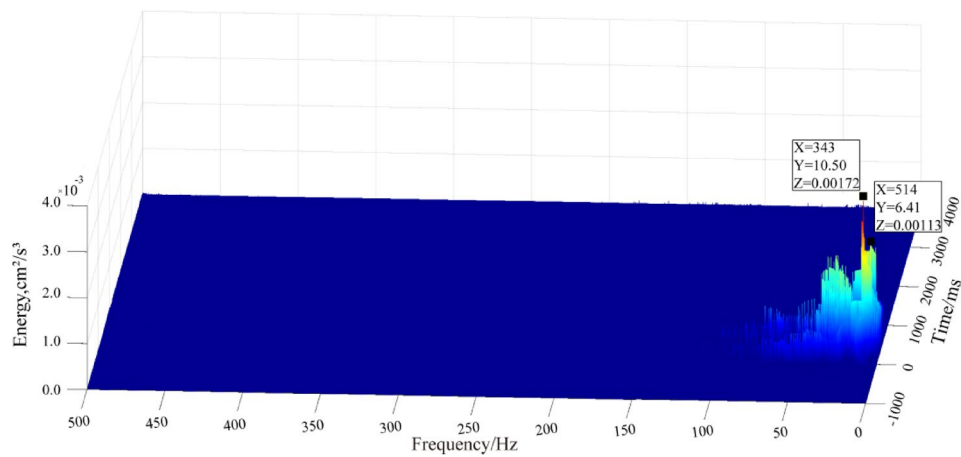


**Fig. 17.** Three dimensional time-frequency energy spectrum of signal.

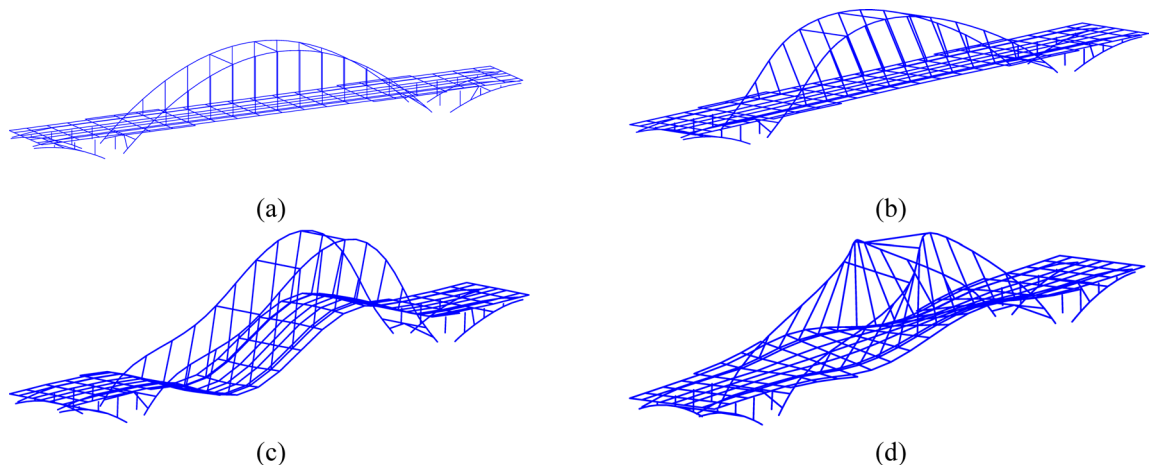


**Fig. 18.** First 3 modes of Liantuo Bridge. (a) Midas calculation model diagram. (b) First order vibration mode diagram. (c) Second order vibration mode diagram. (d) Third order vibration mode diagram.

Formation	Natural frequency	Formation	Natural frequency	Formation	Natural frequency
1	0.98	2	1.96	3	1.97

**Table 1.** Natural frequency corresponding to the first three modes of Liantuo Bridge (unit: Hz).

is, resonance hazard will occur. The forced vibration of objects is carried out according to a certain specific law, that is, they have different natural frequencies, because of their differences in shape and structure. In order to explore the natural frequency of the building structure, it is necessary to analyze the vibration characteristics of the structure, such as the vibration characteristic frequency and the vibration mode corresponding to the frequency, that is, modal analysis. The modal analysis of Liantuo bridge is carried out through Midas. The Midas calculation model diagram and the first three vibration modes of the main bridge of Liantuo bridge are shown in Fig. 18. The natural frequencies corresponding to each mode are shown in Table 1.

From Table 1, it can be seen that the natural frequency of Liantuo Bridge is very small, below 2 Hz. From Fig. 17, it can be observed that the ratio of the energy carried by the blasting seismic wave in the 0–2 Hz frequency band to the total energy is very small and almost negligible. According to the knowledge of structural earthquake resistance, the seismic wave signal generated by this blasting will not cause resonance in Liantuo Bridge.

In conclusion, it can be found that the time-frequency analysis method of underwater blasting seismic wave signal based on DEP-CEEMDAN-MPE-INHT is not only helpful to suppress the modal confusion and endpoint divergence of EMD caused by noisy monitoring signals, but also the time-frequency spectrum obtained by INHT of IMF obtained by DEP-CEEMDAN-MPE has high resolution in time domain and frequency domain. The time-frequency analysis results of the measured noisy blasting seismic wave monitoring signal are consistent with the time-frequency analysis results of the simulated noisy vibration signal, which indirectly reflects the effectiveness and rationality of the DEP-CEEMDAN-MPE-INHT time-frequency analysis algorithm.

Overall, it is not difficult to find. The DEP-CEEMDAN-MPE-INHT algorithm can accurately extract the time-frequency characteristic parameters of the measured noisy blasting seismic wave monitoring signal, contribute to the control of blasting vibration hazards, and play a guiding role in formulating scientific seismic measures.

## Discussion

The proposed DEP-CEEMDAN-MPE-INHT algorithm demonstrates significant improvements in time-frequency analysis of blasting seismic waves by addressing three critical challenges of conventional HHT: mode confusion, endpoint effects, and Bedrosian theorem constraints.

## Key advantages

(1) Robust Noise Suppression: The CEEMDAN-MPE combination effectively separates high-frequency noise (via MPE's entropy thresholding) and low-frequency trends (via CEEMDAN), yielding cleaner IMFs (Fig. 5b vs. a).

In simulated tests, the algorithm extracted a 70 Hz amplitude modulation/frequency modulation signal and 15 Hz sinusoid from noisy data (Fig. 6b), while HHT failed due to mode mixing (Fig. 6a).

(2) Endpoint Effect Mitigation: DEP's dual-level energy matching reduced boundary divergence in IMFs.

(3) Physically Meaningful Time-Frequency Resolution: INHT normalized IMFs to avoid negative frequencies, enabling high-resolution time-frequency spectra (Figs. 10, 11, 12, 13, 14, 15, 16 and 17).

## Limitations and future improvements

(1) Parameter Sensitivity: The MPE entropy threshold requires empirical calibration for different blast types. The future plan is to use machine learning to automatically select thresholds.

(2) Generalizability: Validated primarily for blasting seismic waves. Extension to other non-stationary signals requires additional verification.

(3) Adaptive white noise dynamic frequency adjustment: Based on the local signal-to-noise ratio of the signal, adaptively adjust the  $j$  value.

(4) Hardware Deployment: Field deployment on edge devices necessitates further code optimization. Blast design optimization.

## Conclusions

This study proposes the DEP-CEEMDAN-MPE-INHT algorithm to improve time-frequency analysis of noisy blasting seismic wave signals, addressing key limitations of the traditional HHT. The main conclusions are as follows:

(1) DEP-CEEMDAN-MPE-INHT comprehensively considers the problems encountered in HHT algorithm in processing noisy blasting seismic wave signals, and improves them one by one. The EMD mode confusion and endpoint effect suppression are realized, and the Hilbert transform is free from the constraints of Bedrosian theorem, so as to improve the time-frequency analysis accuracy of the noisy blasting seismic wave monitoring signal.

(2) The time-frequency analysis method of the noisy blasting seismic wave monitoring signal based on DEP-CEEMDAN-MPE-INHT not only helps to suppress EMD mode confusion and endpoint divergence caused by noisy monitoring signal, but also the time spectrum obtained by normalized Hilbert transform of IMF obtained by DEP-CEEMDAN-MPE has high resolution in time domain and frequency domain. It is helpful to identify the vibration characteristics of the noisy blasting seismic wave monitoring signal.

## Data availability

All data generated or analysed during this study are included in this published article.

Received: 23 December 2024; Accepted: 3 September 2025

Published online: 07 October 2025

## References

1. Liu, X. et al. Experimental analysis of rotating bridge structural responses to existing railway train loads via time-frequency and Hilbert-Huang transform energy spectral analysis. *Sci. Rep.* **14** (1). <https://doi.org/10.1038/s41598-024-58795-0> (2024).
2. Sun, M. et al. Smooth model of blasting seismic wave signal denoising based on two-stage denoising algorithm. *Geosyst Eng.* **23** (04), 234–242 (2020).
3. Han, Z. et al. The time-frequency analysis of the acoustic signal produced in underwater discharges based on variational mode decomposition and Hilbert-Huang transform. *Sci. Rep.* <https://doi.org/10.1038/s41598-022-27359-5> (2024).
4. Chen, G. et al. Main frequency band of blast vibration signal based on wavelet packet transform. *Appl. Math. Model.* **74**, 569–585 (2019).
5. Huang, D. et al. Wavelet packet analysis of blasting vibration signal of mountain tunnel. *Soil Dyn. Earthq. Eng.* **117**, 72–80 (2019).
6. Zhao, M. S. et al. Time-frequency characteristics of blasting vibration signals measured in milliseconds. *Min. Sci. Technol. (China)*. **21** (3), 4 (2011).
7. Huang, N. E. A review on Hilbert-Huang transform: method and its application to geophysical studies. *Rev. Geophys.* **46**, 1–23 (2008).
8. Daryan, A. S. et al. A modal nonlinear static analysis method for assessment of structures under blast loading. *J. Vib. Control.* **24**, 3631–3640 (2018).
9. Wang, T. et al. Comparing the applications of EMD and EEMD on time-frequency analysis of seismic signal. *J. Appl. Geophys.* **83** (29–34), 29–34 (2012).
10. Huang, N. E. et al. The empirical mode decomposition and the Hilbert spectrum for nonlinear and non-stationary time series analysis[J]. *Proceedings A*, 454(3): 903–995. (1998).
11. Huang, N. E. et al. A new view of nonlinear water waves: the hilbert spectrum[J]. *Annu. Rev. Fluid Mech.* **31** (1), 417–457 (1999).
12. Wu, J. et al. Analysis and research on blasting network delay of Deep-Buried diversion tunnel crossing fault zone based on EP-CEEMDAN-INHT. *Geotech. Geol. Eng.* **40** (3), 1363–1372 (2022).
13. Fang, C. et al. Denoising method of machine tool vibration signal based on variational mode decomposition and Whale-Tabu optimization algorithm. *Sci. Rep.* [10.1038/s41598-023-28404-7](https://doi.org/10.1038/s41598-023-28404-7) (2024).
14. Peng, Y. X. et al. A novel denoising model of underwater drilling and blasting vibration signal based on CEEMDAN. *Arab. J. Sci. Eng.* **46**, 4857–4865 (2021).
15. Wu, Q. et al. Boundary extension17 and stop criteria for empirical mode decomposition. *Adv. Adapt. Data Anal.* **2**, 10–43 (2014).
16. Yao, G. et al. Separation of systematic error based on improved EMD method. *J. Vib. Shock.* **33**, 176–180 (2014).
17. Wang, B. X. et al. Bridge vibration signal optimization filtering method based on improved CEEMDAN-multiple-scale permutation entropy analysis. *Journal Jilin University (Engineering Technol. Edition)*. **50**, 216–226 (2020).
18. Yeh, J. R. et al. Complementary ensemble empirical mode decomposition: a novel noise enhanced data analysis method. *Adv. Adapt. Data Anal.* **2**, 35–156 (2010).
19. Sun, M. et al. Time-frequency analysis of blasting seismic signal based on CEEMDAN. *Journal South. China Univ. Technology (Natural Sci. Edition)*. **48** (03), 76–82 (2020).
20. Rao, X. et al. Identification of the blasting vibration characteristics of groundwater-sealed tunnel. *Scientific Reports*, **13**(1), 13557 <https://doi.org/10.1038/s41598-023-40728-y> (2023).
21. Huang, N. E. ON instantaneous frequency. *Adv. Adapt. Data Anal.* **1** (02), 177–229 (2009).

## Acknowledgements

Thanks for the help of Junkai Yang. He offered advice on the composition and technical support on the numerical modeling of the article.

## Author contributions

Conceptualization, S.M., and W.J.; methodology, S.M.; software, S.M., and W.J.; validation, S.M., L.Y., and Y.F.; data curation, S.M., and W.Y.; writing original draft preparation, S.M. and W.J.; writing review and editing, S.M., and W.Y.; funding acquisition, L.Y., S.M., and W.J.; All authors have read and agreed to the published version of the manuscript.

## Funding

This research was funded by the National Natural Science Foundation of China, 41907259; and the Foundation of Research Center of Hubei Small Town Development, 2024A004; the Natural Science Foundation of Hubei Province of China, 2022CFB948; and the Foundation of Engineering Research Center of Rock-Soil Drilling & Excavation and Protection, 202404 and 202409. This research was supported by the Key project of Scientific Research Plan of Hubei Provincial Department of Education (Grant No. D20242702), which is administered by the corresponding author, Dr. Jing Wu.

## Declarations

### Competing interests

The authors declare no competing interests.

### Additional information

**Correspondence** and requests for materials should be addressed to J.W.

**Reprints and permissions information** is available at [www.nature.com/reprints](http://www.nature.com/reprints).

**Publisher's note** Springer Nature remains neutral with regard to jurisdictional claims in published maps and institutional affiliations.

**Open Access** This article is licensed under a Creative Commons Attribution-NonCommercial-NoDerivatives 4.0 International License, which permits any non-commercial use, sharing, distribution and reproduction in any medium or format, as long as you give appropriate credit to the original author(s) and the source, provide a link to the Creative Commons licence, and indicate if you modified the licensed material. You do not have permission under this licence to share adapted material derived from this article or parts of it. The images or other third party material in this article are included in the article's Creative Commons licence, unless indicated otherwise in a credit line to the material. If material is not included in the article's Creative Commons licence and your intended use is not permitted by statutory regulation or exceeds the permitted use, you will need to obtain permission directly from the copyright holder. To view a copy of this licence, visit <http://creativecommons.org/licenses/by-nc-nd/4.0/>.

© The Author(s) 2025